

CHARACTERIZATION OF THE SR VISIBLE BEAM POLARIZATION STATE AT SPEAR3[†]

Chunlei Li¹, Jeff Corbett² and Toshiyuki Mistuhashi³

¹East China University of Science and Technology, Shanghai, China

²SLAC National Accelerator Laboratory, Menlo Park, USA

³KEK, Tsukuba, Japan

Abstract

Synchrotron radiation has the well-known property of horizontal field polarization in the midplane with increasingly elliptical polarization in the vertical plane. By measuring the beam intensity transmitted through a linear polarizer, it is possible to characterize the beam polarization state, determine the Stokes' parameters and solve for the beam polarization ellipse in the visible portion of the SR spectrum. The results can be compared with Schwinger's equations for synchrotron radiation taking into account the effect of extraction mirrors.

INTRODUCTION

Synchrotron radiation (SR) has both partially-coherent and fully-polarized electromagnetic field properties, each used for a wide range of scientific research. With the advent of high-power, short-pulse free-electron lasers, applications depending on the spatial beam coherence are growing at a rapid rate. Similarly elliptically polarized x-rays have become an increasingly powerful tool to study magnetic dichroism and chirality at both storage rings and FEL facilities [1]. The large vertical opening angle of visible light in the diagnostic beam line at SPEAR3 provides a unique opportunity to study both the transverse spatial coherence [2] and electromagnetic polarization state of the beam [3].

The polarization state in particular can be characterized by measuring beam power transmitted through a polarizer oriented at systematic angles with respect to the x-y beam axis. In this way it is possible to obtain 'slice' measurements of the beam polarization ellipse which can be combined to represent the beam polarization state in terms of the Stokes parameters [3,4].

To cross-check the measurements we compare with Schwinger's equations for the SR field [5]. These 'classical' equations express the horizontal and vertical field intensities $E_x^2(\omega, \psi)$ and $E_y^2(\omega, \psi)$ in terms of radiation frequency ω and, conveniently, vertical observation angle ψ . For SR the relative phase difference between E_x and E_y is $\pm\delta=\pi/2$ at all emission angles depending on whether the observer is above (+) or below (-) the midplane, and $E_x \neq E_y$, so the radiation is in general elliptically polarized. Using the SPEAR diagnostic beam line it is possible to measure and calculate the SR polarization state in the visible light regime as a function of vertical observation angle.

[†]Work sponsored by U.S. Department of Energy, Office of Basic Energy Sciences under Contract No. DE-AC02-76SF00515 and the China Scholarship Council. corbett@slac.stanford.edu

MEASUREMENT SYSTEM

Figure 1 shows a plan view of the SPEAR3 diagnostic beam line. The beam line contains a horizontal 'cold finger' to block the on-axis hard x-ray SR component followed by a rhodium-coated mirror to horizontally reflect visible dipole radiation into the diagnostic laboratory. The cold finger blocks ± 0.6 mrad of the beam at the midplane and the surrounding apertures have an acceptance of 3.5 mrad \times 6 mrad. A pair of near-incidence Aluminum mirrors is used to reject any stray x-ray Compton scattering and align the SR beam with the optical bench. An image of the $60\text{mm} \times 100\text{mm}$ unfocused visible SR beam showing the shadow of the cold finger at the measurement station is seen in Fig. 2.

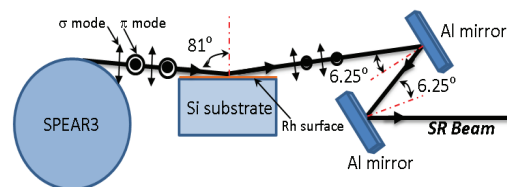


Figure 1: Plan view of the diagnostic beamline.

For the beam polarization measurements, we constructed a remote-controlled scanning system rotatable polarizer, 532nm bandpass filter (BP) and power meter on a continuous-motion vertical stage [6]. An insertable quarter waveplate (QWP) optically matched the bandpass filter is used to determine helicity of the elliptically polarized light.

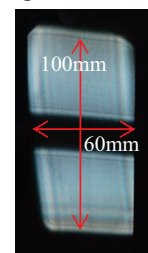


Figure 2: Unfocused visible SR Beam.

As shown in Fig. 3, the polarizer was installed on a computer controlled rotation stage (Newport URS50BPP) to adjust the polarizer axis.

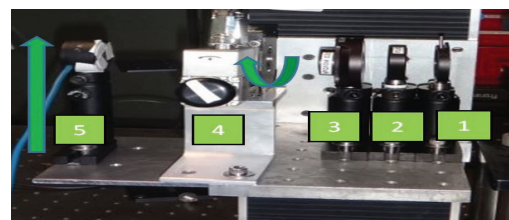


Figure 3: Measurement apparatus: 1-iris, 2-BP filter, 3-quarter wave plate, 4-polarizer, 5- power meter.

remotely. The complete optical system was installed on a vertically-adjustable stage to measure the beam intensity at different observation angles.

The automated measurement system contains two main parts - one for motor control and the other for data acquisition. A block diagram of the system is shown in Fig. 4. The motor control system is composed of 3 components: (1) an SSRL in-house motor controller, (2) an in-house motor driver, and (3) Allied Electronics stepper motor M062-LS03E. The data acquisition system also contains 3 parts: (1) Newport 1815-C power meter with 818-UV sensor, (2) Nova R&D Inc., N101 voltage-to-frequency converter, and (3) in-house counter/timer electronics.

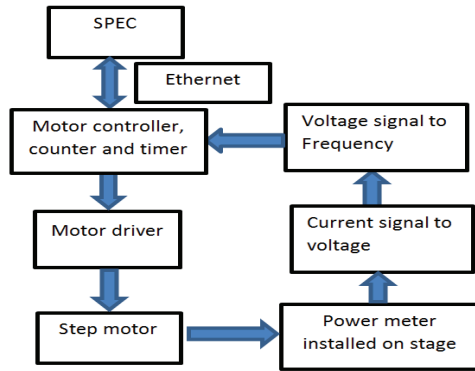


Figure 4: Block diagram for continuous-scan system.

To record beam intensity the Newport 1815-C voltage signal was first converted to a frequency-modulated pulse train through the voltage-to-frequency module. The frequency signal was then detected using the SSRL counter/timer electronics. SPEC software version 6.02.08 (Certified Scientific Software, USA) was used to communicate with both the motor controller and the counter/timer to move the vertical stage at a continuous rate while synchronously collecting intensity data [6].

In general five parameters need to be defined for the trajectory of the vertical stage. They are start position (s), end position (f), number of intervals (n), data acquisition time for each interval (t) and the motor acceleration time (t_{acc}). The distance of each interval can be calculated according to Eq. 1a, and the velocity v calculated from Eq. 1b:

$$d = \frac{f-s}{n} \quad (1a)$$

$$v = \frac{d}{t} \quad (1b)$$

In order to make the detector system move at constant velocity during the measurement process, an acceleration segment d_{acc} and deceleration segment d_{dec} were added before the start and after the end positions. The distance of the acceleration and deceleration segments can be calculated from Eq. 2a. The start position s_{start} and end position s_{end} of the acceleration part are calculated from Eqs. 2b-c, and the deceleration part from Eqs. 2d-e.

$$d_{acc} = d_{dec} = 0.5 \times v \times t_{acc} \quad (2a)$$

$$s_{start} = s - 0.5 \times d - d_{acc} \quad (2b)$$

$$s_{end} = s - 0.5 \times d \quad (2c)$$

$$s_{start} = f + 0.5 \times d \quad (2d)$$

$$s_{end} = f + 0.5 \times d + d_{dec} \quad (2e)$$

BEAM LINE MIRROR EFFECTS

The first optical element in the SR beam line is the rhodium-coated pickoff mirror. Due to geometric constraints, the mirror intercepts the SR beam at a steep incidence angle of 81° to the surface normal [7]. The reflected field attenuation and phase shift can be calculated from Fresnel's laws [8]

$$r_s = \frac{R_s}{E_s} = \frac{n_1 \cos \theta_i - n_2 \cos \theta_t}{n_1 \cos \theta_i + n_2 \cos \theta_t} \quad (3a)$$

$$r_p = \frac{R_p}{E_p} = \frac{n_2 \cos \theta_i - n_1 \cos \theta_t}{n_1 \cos \theta_t + n_2 \cos \theta_i} \quad (3b)$$

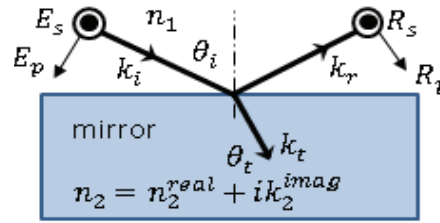


Figure 5: S- and P-wave reflection at a mirror surface.

where as seen in Fig. 5 E_s, E_p and R_s, R_p are the incident and reflected electric field values, respectively, $n_1=1$ is the free-space index of refraction, and n_2 is the complex-valued refractive index for the mirror. θ_i and θ_t (complex) are related by Snell's law:

$$n_1 \sin \theta_i = n_2 \sin \theta_t \quad (3c)$$

Of note horizontally-polarized σ -mode SR radiation corresponds to the P-polarized field component at the horizontally reflecting Rh mirror in the parlance of optics (parallel to the plane of incidence). Similarly, π -mode SR radiation corresponds to the S-polarization component at the mirror. Designations $\{\sigma, \pi\} = \{P, S\}$ will be used in context below for consistency with both nomenclatures.

Table 1 lists the complex refractive index value n_2 and calculated reflectivities r_s and r_p for the Rh mirror at 81° incidence angle at three different wavelengths. Also shown are the ratios for intensity reflectance $I_p/I_s = (r_p/r_s)^2$ and net phase shift $\Delta\phi_{s/p}$ between field components E_s and E_p . According to the calculation, the ratio I_p/I_s is ~ 0.5 indicating the intensity of the SR σ component should be attenuated twice as much as the π component due to optical activity of the rhodium mirror.

Figure 6 shows a plot of intensity reflectance for the S and P polarization components as a function of incidence angle on the Rh surface at $\lambda=532\text{nm}$ [9]. At an incidence angle of 81° the P-polarization reflectance is near the minimum value.

Table 1: Rh mirror reflection parameters at 81° incidence. $\Delta\phi_s$ and $\Delta\phi_p$ are phase change of S and P waves at the mirror surface. $\Delta\phi_{s/p}$ is the net phase change (see Fig. 7).

Wavelength (nm)	430	532	650	
Refractive index	1.64	1.93	2.19	
Extinction index	4.37	4.89	5.74	
Reflectivity	r_s	0.98	0.98	0.98
	r_p	0.70	0.68	0.68
	I_p/I_s	0.51	0.48	0.48
Reflection phase	$\Delta\phi_s$	-176.4°	-176.9°	-177.3°
	$\Delta\phi_p$	-70.1°	-77.2°	-87.0°
	$\Delta\phi_{s/p}$	-16.3°	-9.7°	-0.3°

In terms of phase, Table 1 indicates at 532nm the S-wave is delayed by -176.9° and the P-wave is delayed by -77.2°. Figure 7 shows how the delays act on the two polarization components. As pictured, the S-wave (π -mode) begins 90° ahead of the P-wave prior to reflection. After reflection the S-wave is 10° behind the P-wave so that light is more linearly polarized and the helicity reversed. On the opposite side of the midplane the S-wave leads the P-wave by 170° after reflection.

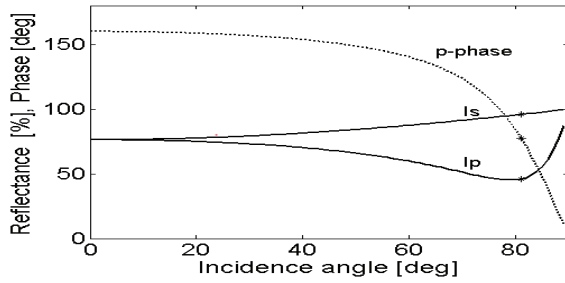


Figure 6: Calculated intensity reflectance for S and P waves at the Rh mirror for $\lambda=532\text{nm}$. Dashed line is the phase retardation for P-waves.

The net effect of the Al mirrors is to produce a reflectance ratio I_p/I_s near unity and relative phase shift of order 1° for visible light.

STOKES LAW AND THE BEAM POLARIZATION ELLIPSE

At optical and x-ray frequencies oscillations of the electromagnetic field are too fast for direct measurement. Detectors can only record beam intensity $I = EE^*$ and phase information is lost. This problem has confounded scientists for centuries. In a seminal paper published in 1852, G.G. Stokes proposed a theoretical framework to characterize the polarization state of light without direct measurement of the oscillating field [10]. The measurements require use of a single polarizing element in conjunction with a phase retarder (waveplate). For our application, when the SR beam passes through a polarizer oriented at angle θ with respect to the x-axis, the transmitted field is

$$E = E_{x0} \cos \theta + E_{y0} \sin \theta e^{i\delta} \quad (4)$$

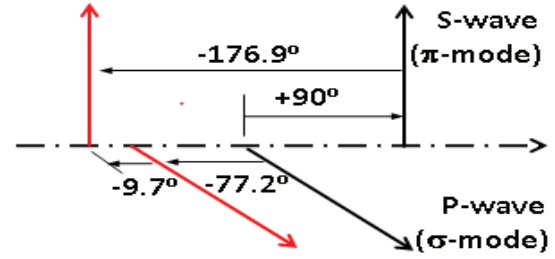


Figure 7: Electric field phase shift at the Rh mirror. S-wave is +90° at incidence and -10° after reflection.

where E_{x0} and E_{y0} are the Cartesian field amplitudes and δ the relative phase difference. Substituting E into $I = EE^*$ yields a simplified version of Stokes' Law for beam intensity as a function of polarizer angle θ in the absence of a phase retarder:

$$I(\theta) = E_{x0}^2 \cos^2 \theta + E_{y0}^2 \sin^2 \theta + 2E_{x0}E_{y0} \cos \theta \sin \theta \cos \delta \quad (5)$$

Examination of Eq. 5 reveals that three field parameters $\{E_{x0}, E_{y0}, \delta\}$ are sufficient to describe the basic polarization state of the SR beam. Knowledge of these three parameters also provides a graphical representation in terms of the beam polarization ellipse:

$$\frac{E_x^2}{E_{x0}^2} - 2 \frac{E_x E_y}{E_{x0} E_{y0}} \cos \delta + \frac{E_y^2}{E_{y0}^2} = \sin^2 \delta \quad (6)$$

The polarization ellipse is a statistically time-average quantity that is readily derived by eliminating the propagator term $\omega t - kz$ from parametric plane wave expressions for E_x and E_y , namely [4]

$$E_x = E_{x0} e^{-i(\omega t - kz + \delta)} \quad (7a)$$

$$E_y = E_{y0} e^{-i(\omega t - kz)} \quad (7b)$$

where again δ is the relative phase between E_x and E_y . For SR radiation E_{x0} and E_{y0} obey Schwinger's equations as a function of ω and vertical observation angle ψ . Mathematically the beam polarization ellipse is closely related to the intensity modulation curve in Eq. 5 but provides a more intuitive picture of the field polarization characteristic.

From Stokes Law, the first three Stokes parameters can be recovered by recording beam intensity without the QWP in place and the polarizer oriented at angles $\theta=0^\circ, 45^\circ, 90^\circ$ and 135° with respect to the x-axis. By definition of the Stokes parameters and inspection of Eq. 5 we have

$$S_0 = I_{0^\circ} + I_{90^\circ} = E_{x0}^2 + E_{y0}^2 \quad (8a)$$

$$S_1 = I_{0^\circ} - I_{90^\circ} = E_{x0}^2 - E_{y0}^2 \quad (8b)$$

$$S_2 = I_{45^\circ} - I_{135^\circ} = 2E_{x0}E_{y0} \cos \delta \quad (8c)$$

As demonstrated in [3], measurements of I_{0° and I_{90° yield E_{x0} and E_{y0} which can be used to calculate the phase parameter δ from Eq. 8c.

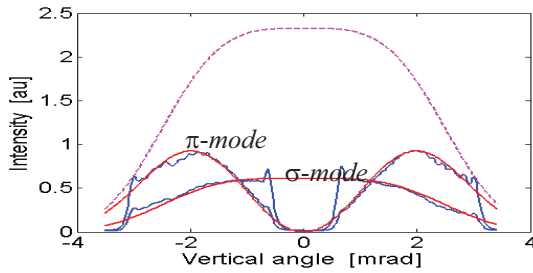


Figure 8: Horizontal (σ -mode) and vertical (π -mode) polarization intensities vs. vertical observation angle. Blue=measured, red=model, magenta=free space.

Introduction of the quarter waveplate yields the forth Stokes parameter (S_3) associated with right/left 'handedness' of the electromagnetic field polarization:

$$S_3 = I_{45^\circ}^{QWP} - I_{135^\circ}^{QWP} = 2E_{x0}E_{y0}\sin\delta \quad (8d)$$

where the superscript QWP indicates the quarter waveplate has been inserted with fast axis oriented along one of the principle x-y axes.

MEASUREMENTS AT 532nm

Figure 8 shows the measured SR polarization intensities E_{x0}^2 and E_{y0}^2 as a function of vertical elevation angle. Compared with Ref. [3], the data spans a larger vertical observation angle and the storage ring vacuum chamber has been re-aligned to reduce edge diffraction at the limiting apertures. Some diffraction at the top, bottom and cold finger is still apparent.

Calculated beam intensity curves based on Schwinger's equations are superimposed on the data. For the σ -mode calculation, the curve was reduced by a factor of 0.26 relative to the calculated value. Referring to Table 1, the anticipated reduction due to the Rh mirror is only 0.50. The difference may be attributed to electro-chemical coating of the Rh mirror surface after years of SR fluence altering the complex index of refraction. The *un-scaled* theoretical σ -mode curve is shown as a dashed line.

Figure 9 shows the measured beam intensities with the polarizer oriented at 45° and 135° . Substituting the Schwinger model for field values E_{x0} and E_{y0} deduced from Fig. 8 into the expression for field projection Eq. 4, the model beam intensities were again calculated for polarizer angles of 45° and 135° . In this case, the relative phase angle δ was set to 10° to account for optical activity at the Rh mirror (see Table 1). The dashed line shows the theoretical result in the absence of the Rh mirror, i.e. no beam attenuation and $\delta = \pi/2$.

Notably for both the top and bottom segments of the SR beam the beam intensity changes dramatically as the polarizer is rotated from 45° to 135° . This is indicative of a near-linear polarization state of the light. The result is consistent with a small phase angle δ between the

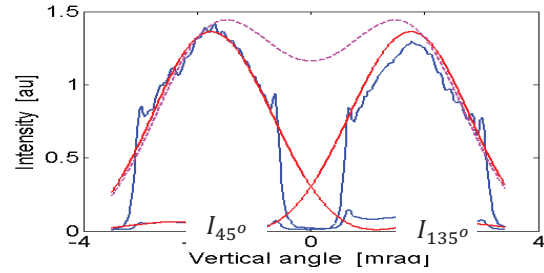


Figure 9: Beam intensity measured with polarizer oriented 45° and 135° . Blue=measured, red=model magenta=free space.

σ and π mode radiation components after reflection.

The beam polarization ellipse at 1mrad vertical observation angle is plotted in Fig. 10 to demonstrate the near-linear polarization state with the major axis of the ellipse much larger than the minor axis. Referring to Fig. 8, at 1mrad the horizontal and vertical fields are approximately equal. The large magenta ellipse plotted in Fig. 10 is the free-space result predicted from Schwinger's equations in front of the mirror.

In this case the horizontal field amplitude is a factor of two more than the vertical field and the ellipse is upright because the free-space SR phase angle $\delta=90^\circ$.

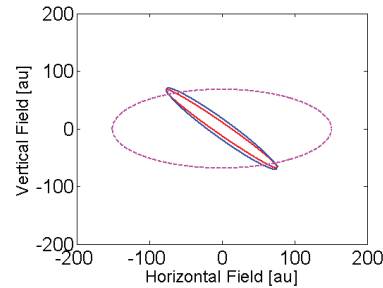


Figure 10: Beam polarization ellipse at $\psi=1\text{mrad}$. Blue=measured, red=model, magenta=free space.

In order to analyse polarization helicity, recall quarter waveplates can convert linearly polarized light into circular polarized light and vice versa. In our case the quarter waveplate was inserted with fast axis aligned vertical so the horizontal σ -mode light was delayed 90° .

Following the prescription for measurement of S_3 (Eq. 8d) the polarizer was again oriented at 45° and 135° and vertical scans of beam intensity recorded. Both the raw data and the calculated curves based on Schwinger's model are plotted in Fig. 11, again using the model phase angle of $\delta=10^\circ$. The different between the 45° and 135° data yields polarization helicity.

As expected, the phase retarding effect of the QWP causes the polarization state to change from a near-linear condition (Figs. 9,10) to a more circular state, i.e. the length of major and minor axes of the beam polarization ellipse are now more equal in magnitude and the relative phase between E_x and E_y is closer to 90° . The data again

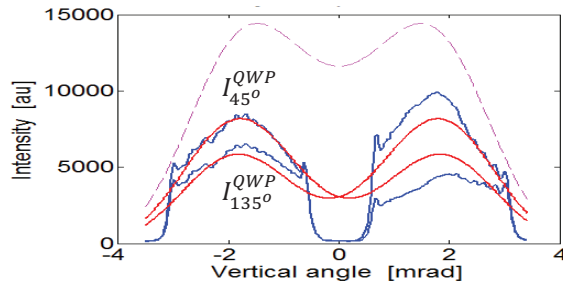


Figure 11: Beam intensity measured with QWP installed and polarizer oriented 45° and 135° . Blue=measured, red=theory, magenta=free-space.

shows an asymmetry between the top and bottom portions of the beam. The cause of the asymmetry is under investigation.

PHASE SHIFT AT THE Rh MIRROR

To further analyse the top/bottom asymmetry we can calculate the relative phase shift δ between the polarization components directly from the measured data. In this case the field amplitudes E_x and E_y are derived from the σ - and π -mode intensity measurements in Fig. 8, this time using the raw data instead of the model. These values are again substituted into the Eq. 8c where measured data is also used for $I_{45^\circ} - I_{135^\circ}$ to solve for the phase angle δ . As seen in Fig. 12, this method yields a phase factor $\delta \sim -15^\circ$ in the bottom half of the beam, close to the calculated value of $\delta = -9.7^\circ$. (Without the Rh mirror the phase differential would be $\delta = +90^\circ$.) The resulting 'measured' beam polarization ellipse is superimposed on the calculated ellipse in Fig. 10. The measured ellipse is slightly more 'elliptical' because the phase angle δ is larger.

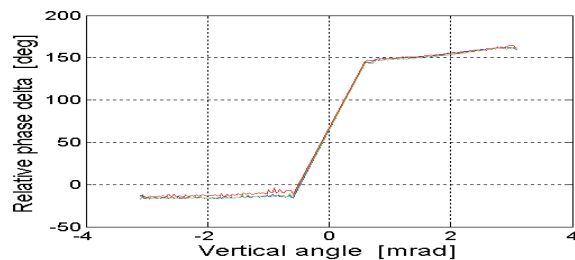


Figure 12: Relative phase angle δ between σ -mode and π -mode polarization components after Rh mirror. Blue: 430nm, green: 532nm, red: 650nm.

Figure 12 also shows the result of the same calculation process applied to data recorded with 430nm and 650nm bandpass filters. In the lower portion of the beam the measured phase is near the calculated value but does not show the trend toward $\delta = 0^\circ$ seen in Table 1 at longer wavelengths. Since the phase angle is a sensitive function of incidence angle the measurements are nonetheless considered plausible. In the upper portion of the beam the phase is observed to change with the vertical elevation angle indicating either surface contamination or more likely physical distortion of the mirror surface.

CONCLUSIONS

Beam polarization measurements at the SPEAR3 diagnostic beam line were evaluated taking into account both field attenuation and phase shift of the SR beam at the Rhodium pickoff mirror. The vertical beam polarization profile is found to be in good agreement with Schwinger's theory for highly relativistic synchrotron radiation emission. A factor of 2 anomaly in reflectance is observed leading to a larger than expected reduction in the σ -mode component. Accepting the validity of Schwinger's equations in the visible regime we attribute the difference to as-yet unexplained optical activity at the surface of the pickoff mirror.

The relative phase between E_x and E_y is close to the predicted value after reflection from the Rh mirror leading toward a more linear polarized beam than the free-space SR beam condition before the mirror. Across the bottom surface of the mirror the relative phase is nearly constant as anticipated. The phase shift slews across the top of the mirror indicating a possible physical distortion of the mirror.

ACKNOWLEDGMENTS

The authors would like to thank the China Scholarship Council, A.Knowles, D.Van Campen, M.Polyanskiy, W.J.Zhang, and SPEAR3 staff for support of this work.

REFERENCES

- [1] R. Kukreja, et al., *X-rays Expose Transparent Spins*, Physical Review Letters, 24 August 2015.
- [2] T.Mitsuhashi, *Measurements using Spatial Coherence of SR*, IPAC15, Richmond, VA (2015).
- [3] J.Corbett, C.L.Li, et al., *Characterization of Visible SR at SPEAR3*, IPAC15, Richmond, VA (2015).
- [4] E.Collett, *Polarized Light: Fundamentals and Applications*, Marcel Dekker, Inc., NY (1992).
- [5] A.Hoffmann, *The Physics of Synchrotron Radiation*, Cambridge University Press (2004)
- [6] C.L.Li, A.M.Kiss and W.J.Zhang, *Investigation of Continuous Scan Methods for Rapid Data Acquisition*, IPAC15, Richmond, VA (2015).
- [7] C.Limborg, et al., *An Ultraviolet Light Monitor for SPEAR3*, EPAC02, Paris, France (2002).
- [8] E.Hecht, *Optics*, 2nd Edition, Addison-Wesley (1987).
- [9] A useful calculator for reflectivity at mirror surfaces can be found at <http://refractiveindex.info/>
- [10] G.G. Stokes, *On the Composition and Resolution of Streams of Polarized Light from Different Sources*, Trans. Camb. Phil. Soc., Vol. IX, 399 (1852).